Preparation of $NaYF_4:Er^{3+}/TiO_2$ composite and up-conversion luminescence properties under visible light excitation*

Ye Yan-Xi(叶岩溪)[a)c)], Hu Xiao-Yun(胡晓云)[a)c)†], Yan Zhi-Yun(闫志云)[a)], Liu En-Zhou(刘恩周)[b)], Fan Jun(樊 君)[b)], Zhang De-Kai(张德恺)[a)], Miao Hui(苗 慧)[a)], Shang Yi-Bo(商毅博)[a)], and Yang Juan(杨 娟)[a)]

[a)] *Department of Physics, Northwest University, Xi'an* 710069, *China*
[b)] *School of Chemical Engineering, Northwest University, Xi'an* 710069, *China*
[c)] *National Photoelectric Technology and Functional Materials & Application of Science and Technology for International Cooperation Base, Northwest University, Xi'an* 710069, *China*

(Received 7 December 2010; revised manuscript received 22 March 2011)

The up-conversion luminescence composite $NaYF_4:Er^{3+}/TiO_2$ is prepared using the sol–gel method. The specimen has good crystallinity and two shapes, i.e., viereck and round, while the sizes of viereck and round particles are both micron-sized. The TiO_2 has an anatase structure, while the $NaYF_4$ has a hexagonal phase, which can be hardly obtained through the common sol–gel method. Due to the big particle size and the high crystallinity of pure $NaYF_4:Er^{3+}$, the composite has a small specific surface area that is less than Degussa P25 TiO_2. The $NaYF_4:Er^{3+}/TiO_2$ composite shows several emission peaks at 211, 237, and 251 nm under the excitation of 388 nm, at 395 nm and 411 nm under the excitation of 500 nm, and at 467, 481, 492, and 508 nm under the excitation of 570 nm.

Keywords: up-conversion luminescence, $NaYF_4:Er^{3+}/TiO_2$ composite, excitation of visible light

PACS: 78.55.–m, 77.84.Lf, 32.80.Rm **DOI:** 10.1088/1674-1056/20/8/087803

1. Introduction

Recently, up-conversion luminescence phosphors (UCPs) have attracted great interest due to their application in areas such as tunable infrared phosphors for three-dimensional optical recording, white light generation for ambient lighting and display, solid-state lasers, solar cells, and biological labels.[1] $NaYF_4:Er^{3+}$ which has been extensively studied and used in many fields, is thought to be one of the highest luminous efficiency UCPs under the excitation of 980 nm emitted by a semiconductor laser.[2−5] Nevertheless, there are few reports on $NaYF_4:Er^{3+}$ emitting ultraviolet, purple, and blue light beams under the excitation of visible light. TiO_2 is highly chemically stable and has strong resistance to wear and innocuity. Consequently, it is the best potential photocatalyst in fields such as photocatalytic decomposition water for hydrogen, the transformation of CO_2 into usable resources, and the decomposition of dye-containing wastewater.[6,7] However, TiO_2, with its wide band gap, can only absorb ultraviolet light that occupies less than 5% of solar energy, leading to its poor photocatalytic performance. A common means of improving its photocatalytic performance is to sensitize the TiO_2 with dye to make it absorb more solar energy, or dope ions into TiO_2 to modify its band gap.[8,9]

In this work, we integrate UCPs with TiO_2 when they are in the gel state. The $NaYF_4:Er^{3+}$ in the combined material absorbs photons of long wavelength and then emits photons of short wavelength, which give TiO_2 better photocatalytic performance.

2. Experiment

To obtain solution A, CH_3COOH was dropwise added into the stirring mixture containing C_4H_9OH and Ti $(OC_4H_9)_4$. The mole ratio of the three was $4.6:7.4:6.4$. At the same time, Y_2O_3 and Er_2O_3 were dissolved in boiling HNO_3, obtaining clear solution a,

*Project supported by the National Natural Science Foundation of China (Grant No. 20876125), the Research Fund for the Doctoral Program of Higher Education of China (Grant No. 20096101110013), and the Northwest University Graduate Cross-Discipline Funds (Grant Nos. 09YJC27, 09YJC24, and 201031).

†Corresponding author. E-mail: hxy3275@nwu.edu.cn

© 2011 Chinese Physical Society and IOP Publishing Ltd

and NaF was dissolved in deionized water, producing solution b. After that, solution a was dropwise added to b at 40 °C, forming the mixed solution B. NaF, Y_2O_3, and Er_2O_3 were taken according to the mole ratio of $80:10:P$. Solution B was cooled at room temperature after having being stirred for some time. Then it was dropwise added to solution A, which had been stirred for a few hours to obtain the mixed solution. After having aged for some hours in the dish, the steady, homogeneous and transparent pale pink sol was obtained. The sol where $NaYF_4:Er^{3+}$ and TiO_2 were mixed evenly was dried in the vacuum drying chamber at 80 °C for some time to obtain pale pink xerogel. Finally, the up-conversion luminescence composite $NaYF_4:Er^{3+}/TiO_2$ was obtained after having been annealed at 500 °C while the mass percentage of $NaYF_4:Er^{3+}$ is 34.5%.

Phase identification was performed via powder X-ray diffraction (XRD) (Rigaku D/MAX-2400) with Cu Kα radiation ($\lambda = 0.154178$ nm). The morphology and elementary composition were characterized by the Quamta400FEG thermal environment scanning electron microscope (SEM). The specific surface area and porosity were tested by the Nova 2000e BET surface area analysis produced by Quantachrome Instruments. Room-temperature excitation and emission spectra were examined with a Hitachi F-7000 fluorescence spectrometer equipped with a continuous 150-W Xe-arc lamp. To compare the intensities of different specimens, the emission spectra were measured with the same instrument parameters (2.5 nm for excitation slit, 2.5 nm for emission slit, and 700-V for PMT voltage).

3. Results and discussion

3.1. Structural and morphological characterization

A structural characterization according to XRD measurement was carried out in the $NaYF_4:Er^{3+}/TiO_2$ composite. The specimen contains three compositions: anatase TiO_2 (101, 200) (JCPDS NO.21-1272), hexagonal phase $NaYF_4:Er^{3+}$(100, 110, 101, 111, 201, 211, 220) (β-$NaYF_4:Er^{3+}$ (JCPDS NO.28-1192)), and $YO_{1.335}$(002) (JCPDS:39-1065) as shown in the XRD pattern of the representative specimen (Fig. 1). The appearance of $YO_{1.335}$ is due to the fact that some Y^{3+} in the $NaYF_4$ reacts with some O^{2-} in the TiO_2 when the crystal habits of both the $NaYF_4$ and TiO_2 are formed. Consequently, XRD not only proves that the specimen is composed of $NaYF_4$ and TiO_2 majorly, but also illustrates that the structural characterization of the specimen has changed a little. Due to the influence of $NaYF_4:Er^{3+}$, no rutile TiO_2 is present when the annealed temperature is 500 °C.

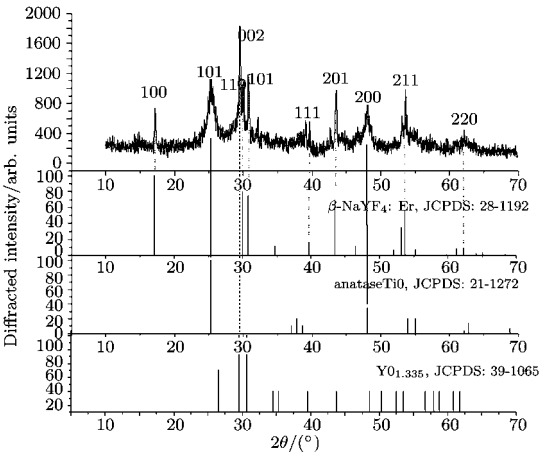


Fig. 1. The XRD patterns of specimen annealed at 500 °C with $P = 2$.

Figure 2 shows the SEM images of two typical specimens. The morphologies of the specimens show that the majority of particles are mainly viereck and a few of them are round while the sizes of both viereck and round particles are both at a micro level. Both morphologies are irregular. The specimen contains some schistose crystals (Fig. 2(a)), which may be the result of $NaYF_4$ and TiO_2 mixing and affecting each other when their crystal habits are formed. The energy dispersive spectrometer (EDS) spectra (Fig. 3) show that the specimen comprises Ti, O, Na, Y, F, and Er elements.

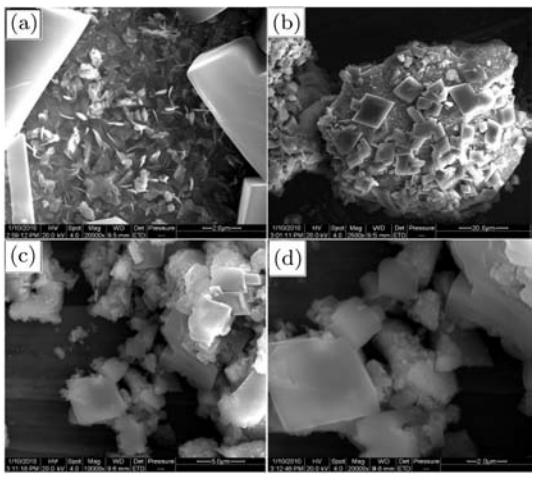


Fig. 2. The SEM images of specimens for $P = 1.5$ [(a) and (b)] and $P = 2$ [(c) and (d)].

Figures 3(a) and 3(b) show that the two specimens have the same elemental compositions. It is not obvious to see that the concentration of Er is a little higher in subplan A. The insets of Figs. 3(a) and 3(b) show the points of the specimens bombarded by electron beams.

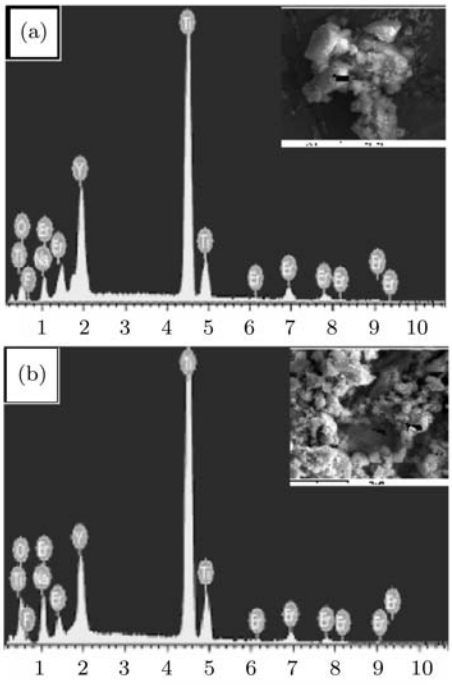


Fig. 3. Energy dispersive spectrometer spectra of specimens for $P = 1.5$ (a) and $P = 2$ (b).

3.2. Specific surface area and porosity of as-prepared $NaYF_4$: Er^{3+}/TiO_2 composite

To recognize further the relation between $NaYF_4$: Er^{3+} and TiO_2 in the specimen, the specific surface areas and porosities of $NaYF_4$: Er^{3+}, TiO_2, and $NaYF_4$: Er^{3+}/TiO_2 composites are tested according to the absorption and the desorption of nitrogen, respectively. The pore diameter is calculated based on the assumption of cylindrical pore geometry by using the Kelvin equation in the form

$$r_{\rm k} = \frac{-2\gamma V{\rm m}}{RT\ \ln(P/P_0)}, \tag{1}$$

where γ is the surface tension of nitrogen at its boiling point, $V_{\rm m}$ is the molar volume of liquid nitrogen, R is the gas constant, T is the boiling point of nitrogen, P/P_0 is the relative pressure of nitrogen, and $r_{\rm k}$ is the Kelvin radius of the pore.

Table 1 summarizes the comparison values of $NaYF_4$: Er^{3+}, TiO_2, and $NaYF_4$: Er^{3+}/TiO_2 composites including specific surface area, average pore diameter, pore volume, and diameter of most of the pores (the detail can be found in Appendix A (a1) and (a2)).

The $NaYF_4$: Er^{3+}, which was also prepared using sol–gel, has a very small specific surface area due to its big particle size (see Appendix A (a3)) and high crystallinity. The specific surface area of the $NaYF_4$: Er^{3+}/TiO_2 composite is between those of $NaYF_4$: Er^{3+} and Degussa P25 TiO_2. In addition, the pore volume and the diameter of most pores of the $NaYF_4$: Er^{3+}/TiO_2 composite are also between those of $NaYF_4$: Er^{3+} and Degussa P25 TiO_2. However, the average pore diameter of the $NaYF_4$: Er^{3+}/TiO_2 composite is bigger than those of both $NaYF_4$: Er^{3+} and Degussa P25 TiO_2. This indicates that the structure of the specimen has changed a little after the $NaYF_4$: Er^{3+} and TiO_2 have been combined, which can be seen from the XRD patterns.

Table 1. Specific surface areas and pore diameters of specimens.

Specimen	$NaYF_4$: Er^{3+}	$NaYF_4$: Er^{3+}/TiO_2 composite	Degussa P25 TiO_2
Specific surface area/(m^2/g)	0.252	16.061	53.641
Average pore diameter/nm	3.427	5.628	3.420
Pore volume/(ml/g)	0.003	0.057	0.194
Diameter of the most pore/nm	17.5	7.2	7.0

3.3. Luminescence of $NaYF_4$: Er^{3+}/TiO_2 composite

Since the $NaYF_4$: Er^{3+} is luminescent material, the $NaYF_4$: Er^{3+}/TiO_2 composite shows nine emission peaks with their maxima at (211, 237, and 251 nm) under the excitation of 388 nm, at (395 and 411 nm) under the excitation of 500 nm, at 467 nm and (481, 492, and 508 nm) under the excitation of 570 nm (Fig. 4). From the energy level of Er^{3+}, according to the calculations, the emission peaks at (211, 237, 251 nm) can be assigned to $^4D_{3/2} \rightarrow {}^4I_{15/2}$ transition because of the $^4D_{3/2}$ level splitting into three states, and (395, 411 nm) can be assigned to $^2H_{9/2} \rightarrow {}^4I_{15/2}$ transition because of the $^2H_{9/2}$ level splitting into two

states. The emission peak at 467 nm has two possible transitions: one is $^2G_{7/2} \rightarrow ^4I_{13/2}$ and the other is $^4F_{5/2} \rightarrow ^4I_{15/2}$ while the (481, 492, 508 nm) can be assigned to $^4F_{7/2} \rightarrow ^4I_{15/2}$.

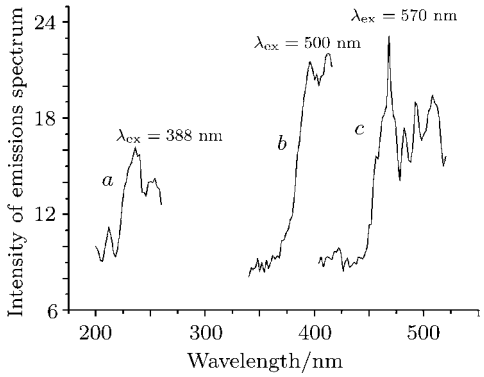


Fig. 4. Emission spectra of $NaYF_4:Er^{3+}/TiO_2$ composite under the excitation of 388 nm (curve *a*), 500 nm (curve *b*), and 570 nm (curve *c*).

Figure 5 shows the energy level diagram of Er^{3+}. The mechanism of the up-conversion luminescence is divided into four: ground slate absorption, GSA/excited state absorption, ESA; energy transfer up-conversion; cooperative up-conversion, and avalanche up-conversion.[10] From the calculation

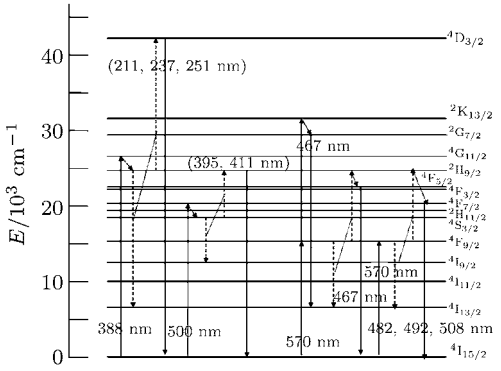


Fig. 5. Energy level diagram of Er^{3+}.

and analysis of excitation wavelength, we speculate the luminescences under the excitations of 388 and 500 nm can belong to the energy transfer up-conversion. They have the energy transfer up-conversion channel[11,12] as follows,

$$\text{Excitation of 388 nm} \begin{cases} {}^4I_{15/2} + h\nu \rightarrow {}^4G_{11/2}, \\ ({}^2G, {}^4F, {}^2H)_{9/2} + {}^2H_{9/2} \rightarrow {}^4I_{13/2} + {}^4D_{3/2}, \\ {}^4D_{3/2} - h\nu \rightarrow {}^4I_{15/2}, \end{cases} \tag{2}$$

$$\text{Excitation of 500 nm} \begin{cases} {}^4I_{15/2} + h\nu \rightarrow {}^4F_{7/2}, \\ {}^4S_{3/2} + {}^4S_{3/2} \rightarrow H_{9/2} + {}^4I_{9/2}, \\ ({}^2G, {}^4F, {}^2H)_{9/2} - h\nu \rightarrow {}^4I_{15/2}, \end{cases} \tag{3}$$

The emission peaks 467 nm and (481, 492, 508 nm) under the excitation of 570 nm can belong to ground slate absorption, GSA/excited state absorption, ESA or energy transfer up-conversion which has two up-conversion channels and energy transfer up-conversion, as follows,

$$\text{Excitation of 570 nm} \begin{cases} \text{channel one} \begin{cases} {}^4I_{15/2} + h\nu \rightarrow {}^4F_{9/2}, \\ {}^4F_{9/2} + h\nu \rightarrow ({}^2P, {}^2D, {}^4F)_{3/2}, \\ {}^2G_{7/2} - h\nu \rightarrow {}^4I_{13/2}, \end{cases} & (4) \\ \text{channel two} \begin{cases} {}^4I_{15/2} + h\nu \rightarrow {}^4F_{9/2}, \\ {}^4F_{9/2} + {}^4F_{9/2} \rightarrow {}^4I_{13/2} + {}^2H_{9/2}, \\ {}^4F_{5/2} - h\nu \rightarrow {}^4I_{15/2}, \end{cases} & (5) \\ \begin{cases} {}^4I_{15/2} + h\nu \rightarrow {}^4F_{9/2}, \\ {}^4F_{9/2} + {}^4F_{9/2} \rightarrow {}^4I_{13/2} + {}^2H_{9/2}, \\ {}^4F_{7/2} - h\nu \rightarrow {}^4I_{15/2}. \end{cases} & (6) \end{cases}$$

4. Conclusion

The up-conversion luminescence composite $NaYF_4:Er^{3+}/TiO_2$ is prepared using the modified sol–gel method. The XRD pattern and SEM images show that the specimen has three compositions: anatase TiO_2, hexagonal phase $NaYF_4$, and

$YO_{1.335}$. The specimen has two types: viereck (majority) and round (minority), while both viereck and round particles are micron-sized. The specific surface area and the porosity show that the structure of $NaYF_4:Er^{3+}/TiO_2$ composite has changed a little after the $NaYF_4:Er^{3+}$ and TiO_2 have been combined. Three ultraviolet emission peaks under the excitation of 388 nm, two purple emission peaks under the excitation of 500 nm, and four blue emission peaks under the excitation of 570 nm are found by the F-7000 fluorescence spectrospece.

Appendix A

(a1) Supporting information about specific surface area for $NaYF_4:Er^{3+}$, TiO_2, and $NaYF_4:Er^{3+}/TiO_2$ composite;

(a2) Supporting information about porosity for $NaYF_4:Er^{3+}$, TiO_2, and $NaYF_4:Er^{3+}/TiO_2$ composite;

(a3) Supporting information about SEM for $NaYF_4:Er^{3+}$.

References

[1] Yanes A C, Santana-Alonso A, Mendez-Ramos J, del-Castillo J and Rodriguez V D 2009 *J. Alloys Compd.* **480** 706

[2] Alexandra R, Janet M, Michael B, Arlete C and Hans J 2006 *Journal of Display Technology* **2** 68

[3] Zhang X L, Wang Y Z and Ju Y L 2005 *Acta Phys. Sin.* **54** 117 (in Chinese)

[4] Tikhomirov V K, Mortier M, Gredin P, Patriarche G, Görller-Walrand C and Moshchalkov V V 2008 *Opt. Soc. Am.* **16** 14544

[5] Zhang F and Zhao D Y 2009 *ACS Nano.* **3** 159

[6] Xu F X, Feng G J, Liu S W, Xiu Z L and Yu J X 2008 *Bull. Chin. Ceram. Soc.* **27** 1140 (in Chinese)

[7] Wang J, Ma T, Zhang G, Zhang Z H, Zhang X D, Jiang Y F, Zhao G and Zhang P 2007 *Catal. Commun.* **8** 607

[8] Hu X Y, Fan J, Chang N, Bai J T and Hou X 2006 *Chem. Engin.* **34** 41 (in Chinese)

[9] Norifusa S, Toshio N, Kenta K and Kimihisa Y 2008 *Nature Nanotechnology* **3** 106

[10] Auzel F 2004 *Chem. Rev.* **104** 139

[11] Chen X B, Li M X, Sawanobori N, Zeng Z and Nie Y X 2000 *Acta Phys. Sin.* **49** 2482 (in Chinese)

[12] Chen X B, Liao H B, Zhang C L, Yu C L, Pan W, Hu L L and Wu Z L 2010 *Acta Phys. Sin.* **59** 5091 (in Chinese)

[13] Liang L F 2005 *Upconversion Properties and Morphology Analysis of* Yb^{3+}/Er^{3+} (*or* Tm^{3+}) *Codoped Fluorides* Ph. D. Thesis (Guangzhou: Sun Yat-Sen University) (in Chinese)

[14] Wang X, Sun X M, Yu D P, Zou B S and Li Y D 2003 *Adv. Mater.* **15** 1442

[15] Alexandra R, Janet M, Michael B, Arlete C and Hans J 2004 *Opt. Soc. Am.* **12** 5215

[16] Qiu J B and Song Z G 2008 *Journal of Rare Earths* **26** 919

[17] Wu C F, Qin W P, Qin G S, Zhao D, Zhang J S, Huang S H, Lu S Z, Liu H Q and Lin H Y 2003 *Appl. Phys. Lett.* **82** 520